

Fibre Optic Sensor for Characterisation of Lithium-Ion Batteries

Jonas Hedman,^[a] David Nilebo,^[b] Elin Larsson Langhammer,^[b] and Fredrik Björefors*^[a]

The interaction between a fibre optic evanescent wave sensor and the positive electrode material, lithium iron phosphate, in a battery cell is presented. The optical–electrochemical combination was investigated in a reflection-based and a transmission-based configuration, both leading to comparable results. Both constant current cycling and cyclic voltammetry were employed to link the optical response to the charge and discharge of the battery cells, and the results demonstrated that the optical signal changed consistently with lithium ion insertion and

extraction. More precisely, cyclic voltammetry showed that the intensity increased when iron was oxidised during charge and then decreased as iron was reduced during discharge. Cyclic voltammetry also revealed that the optical signal remained unchanged when essentially no oxidation or reduction of the electrode material took place. This shows that optical fibre sensors may be used as a way of monitoring state of charge and electrode properties under dynamic conditions.

Introduction

Rechargeable batteries, particularly lithium-ion batteries (LIBs) have emerged as a promising candidate in the pursuit for energy systems to store and deliver energy on demand.^[1] Despite the strong interest and wide use of LIBs in consumer electronics as well as hybrid and electrical vehicles, a complete transition from fossil-fuel-based energy to sustainable energy technologies is challenged by several factors such as insufficient capacity, too short cycle life, high costs, poor low-temperature performance and unexpected failures.^[2,3] Development is also slowed down by lack of adequate techniques for monitoring and understanding harmful chemical processes in the battery systems in real time during cycling, and the need for reliable and more accurate models and control systems for vehicle batteries has increased significantly in recent years.^[2,4] Battery packs in hybrid and electrical vehicles are usually connected in large serial-parallel configurations and coupled with a battery management system (BMS) for monitoring and controlling charging and discharging of the battery, maintaining safe and reliable operation.


A prevailing limitation with current BMSs lies in the difficulty of obtaining the chemical information that describes the state of the battery.^[5,6] At present, information about the battery


state of charge (SOC) and state of health (SOH) is mainly estimated from externally measured temperature, current and voltage.^[6] These parameters are insufficient since they do not provide direct information on the chemical and physical state of the battery during operation nor detailed information of degradation mechanisms. The complexity of LIBs originates from the complicated electrical, chemical and mechanical interplay between the electrodes and electrolyte as well as the interfaces between them as lithium ions are inserted and extracted, making continuous monitoring of the battery state a challenging task. These reactions are highly coupled with each other and influenced by temperature, SOC, cycling procedure and storage conditions.^[3,7] Battery monitoring is also further complicated by ageing processes,^[4,6] making it inherently difficult to monitor and distinguish different degradation and ageing mechanisms from each other and their individual cause dependency.^[5,8]

SOC can be estimated using several methods such as discharge test (not useful for online estimations), coulomb counting involving current integration, open circuit voltage (OCV) evaluation methods or SOC estimation methods based on advanced algorithms and models such as Kalman filters, neural network models and fuzzy logic.^[5,6] SOC estimation methods based on the voltage are accurate and easy to implement but require resting in order for the battery to reach steady state and thus, are not practical during battery operation.^[5,6] Furthermore, OCV only gives a measurement of the cell potential and not the individual electrodes.^[6] A BMS does not usually record information on the individual cell level for practical and economic reasons. Even with improved and sophisticated calculation models current battery management systems have limited capability in predicting battery dynamics and interactions between components in individual cells.^[5] Thus, to maintain safe and reliable performance within the narrow voltage and temperature window in which LIBs operate, the capacity is usually not fully utilised in commercial batteries.

[a] J. Hedman, Dr. F. Björefors
Department of Chemistry - Ångström Laboratory
Uppsala University
Box 538, 751 21 Uppsala (Sweden)
E-mail: Fredrik.bjorefors@kemi.uu.se

[b] D. Nilebo, Dr. E. Larsson Langhammer
Insplorion AB
Arvid Wallgrens backe 20, 413 46 Gothenburg (Sweden)

 Supporting information for this article is available on the WWW under <https://doi.org/10.1002/cssc.202001709>

 © 2020 The Authors. Published by Wiley-VCH GmbH. This is an open access article under the terms of the Creative Commons Attribution Non-Commercial NoDerivs License, which permits use and distribution in any medium, provided the original work is properly cited, the use is non-commercial and no modifications or adaptations are made.

The implementation of fibre optical sensors in LIBs can offer the possibility to separately monitor SOC and SOH without the use of current, voltage and temperature. In addition, optical fibre sensors have several desirable properties such as reduced electromagnetic interference, electrically insulating, small size and lightweight, ability to tolerate chemical conditions as well as remote sensing, real time monitoring and multiplexing capabilities.^[9–11] These properties make them promising for sensor applications in LIBs. Several optical concepts for monitoring battery performance have previously been studied, almost exclusively focusing on graphite electrodes.^[12–14] For example, Xie and Lu studied the extraction of lithium-ions from fully lithiated petroleum coke electrodes using a photometric cell and in situ UV/Vis diffuse reflectance.^[12] Maire et al. used an electrochemical window cell to observe the Li-ion mobility in graphite electrodes during charge and discharge. By correlating the intensities of red, green and blue colour values to lithium content they could approximate an average value of the apparent diffusion coefficient of lithium in graphite.^[13] A similar study by Harris et al. also employed a window cell to observe lithium transport and insertion into graphite electrodes via an optical microscope setup.^[14] They presented a transport model to approximate the lithium diffusion coefficient, which was in reasonable agreement with the observed colour change of graphite upon lithiation. Roscher et al. studied the positive electrode material lithium iron phosphate (LFP) using indium tin oxide (ITO) additives as electrochromic markers in a window cell with in situ video microscopy.^[15] They reported a voltage-dependent reflectivity of the ITO, which correlated with charging and discharging of the LFP/ITO electrode. Other optical methods that have been employed in battery research include Fibre Bragg Grating (FBG) sensors,^[9] to directly measure strain or temperature or to indirectly study intercalation steps or ion diffusion in graphite electrodes through temperature and strain values.^[16–21]

Fibre optical sensors based on the interaction of evanescent waves with surrounding materials are common and have for example been used for measuring the relative humidity,^[22–24] changes in pH^[22,25] or detection of gaseous ammonia, methanol and ethanol^[26–28] as well as hydrogen gas.^[29,30] Evanescent waves have also previously been used within battery research. Ghannoum et al. studied the optical change of extracted commercial graphite electrodes at different SOC using reflectance spectroscopy.^[31] The results were similar to those obtained on petroleum coke by Xie and Lu applying in situ diffuse reflectance.^[12] Graphite electrodes assembled as full cells were also studied with fibre optic evanescent wave spectroscopy in a modified Swagelok cell where a change in transmittance showed a similar behaviour as with the reflectance spectroscopy.^[31] The feasibility of fibre optic evanescent wave sensors in graphite for SOC monitoring was further shown in both Swagelok and pouch cell configurations by the same authors.^[32] In a more recent paper, Ghannoum and Nieva showed the potential use of fibre optic evanescent wave sensors for studying battery degradation.^[33] By taking the slope of the optical transmittance signal during charge cycles, three distinct peaks were found which together with potential-

capacity curves were correlated with intercalation stages in graphite.

In this paper, we report the use of a fibre optic sensor based on evanescent waves for monitoring charge and discharge of lithium iron phosphate in real time. The sensor is fully embedded within the positive electrode in a customised Swagelok cell in both a reflection- and transmission-based fibre optic sensor configuration. The fibre optical measurements were electrochemically coupled with both constant current cycling and cyclic voltammetry (CV) experiments on lithium iron phosphate. The results show that this optical-electrochemical method could potentially be used for SOC estimates. The use of fibre optic sensors in batteries may also reveal additional information about the optical properties of battery materials, which could be useful in battery research and development and could open up new directions within spectroelectrochemistry for studying lithium-ion batteries.

Results and Discussion

For this study, two fibre optical sensor configurations were investigated, a reflection-based fibre optic (RFO) configuration and a transmission-based fibre optic (TFO) configuration. A reflection-based fibre optic sensor is convenient and suitable as it can be miniaturised and inserted relatively easy in a battery with a single entry point, reducing the risk of cell leakage. On the other hand, it increases the complexity of the optical setup as it requires a fibre optic beam splitter to couple light in and out of the same end of the fibre optic sensor probe and direct the output signal to the detector after reflection, which means there is some return loss in the output signal. In this configuration, light is reflected from a metallic mirror deposited at the end face of the fibre optic probe, which might be difficult to manufacture in a highly repeatable and cost effective way, and some light might also escape at the end face if not properly covered. In the TFO configuration, there is no need for an optical beam splitter to separate input and output signals in the optical fibre sensor, simplifying the optical setup and eliminating potential optical effects caused by light interactions with the metallic mirror. The input and output ends of the sensor can be connected with simple fibre optic connectors directly to the light source and the detector, respectively, avoiding loss of light when coupling light in and out of the fibre optic beam splitter. The disadvantage is that in the TFO configuration, the sensor requires access from both sides of the battery cell as it has to be connected to the light source and the detector, complicating implementation since the cell has to be sealed at two entry points. A schematic illustration of the optical-electrochemical experimental setup in the reflection-based configuration is shown in Figure 1 and a photo of the transmission cell configuration is given in Figure S7.

The sensing region of both configurations are based on a pure silica glass rod with a polymer coating. This is different from a standard single or multimode optical fibre, which consists of an optical core surrounded by a cladding where both the core and the cladding are made of silica. A polymer

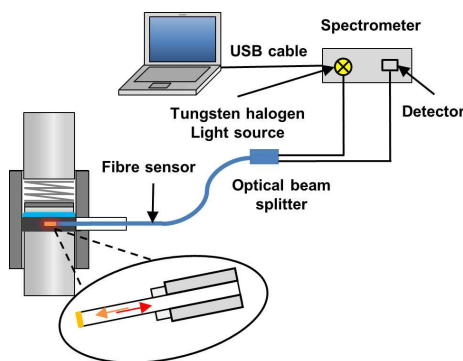


Figure 1. Schematic illustration of the optical–electrochemical experimental setup in the reflection-based configuration.

coating to give the fibre mechanical strength then in turn covers the core and the cladding.

In optical fibres, light guidance occurs by means of total internal reflection (TIR) of the guided rays at the core-cladding interface as the angle of incidence exceeds the critical angle. The core of optical fibres are thus usually doped with germanium or other dopants as to give it a slightly higher refractive index than the cladding.^[34] When light propagates in an optical fibre, it consists of two components: the guided field in the core and the evanescent field extending into the surrounding cladding outside the fibre core. The evanescent field decays exponentially with distance away from the core-cladding interface and falls to almost zero within the cladding. Hence, the evanescent field cannot interact with the surrounding medium in a standard cladded optical fibre. By reducing or completely removing the cladding, the evanescent field is exposed and accessible for interaction with the external medium.^[9,34–36] The field extending into the electrode material is referred to as evanescent since its field strength decreases exponentially with distance z from the core surface into the electrode material according to Equation (1).^[34]

$$E(z) = E_0 \exp\left(\frac{-z}{d_p}\right) \quad (1)$$

where E_0 is the amplitude of the field at the fibre core–electrode interface and d_p is the penetration depth, defined as the distance at which the evanescent field strength falls to $1/e$ of its value at the fibre core–electrode interface. The penetration depth^[34–38] is given by Equation (2):

$$d_p = \frac{\lambda}{2\pi n_1 \sqrt{\sin^2 \theta - \left(\frac{n_2}{n_1}\right)^2}} \quad (2)$$

where λ is the wavelength of the tungsten–halogen light source, n_1 in our case is the refractive index of the pure silica glass rod, n_2 is the refractive index of the surrounding medium (the electrode–electrolyte mixture) and θ the angle of incidence at the pure silica glass rod–electrode interface. The magnitude

of the penetration depth is hence dependent on all these parameters.

Ideally, light is guided in optical fibres with minimal loss through total internal reflection. The coupling of the evanescent field with the surrounding material will, however, result in some loss of electromagnetic energy to the surrounding electrode material through absorption. As a result, there is net energy flow into the surrounding material and light is attenuated, a phenomena known as attenuated total reflection (ATR).^[9,34–37,39–41] The absorption of the evanescent field, which is related to the sensitivity of the sensor, depends on the penetration depth and the number of ray reflections per unit length along the sensing region.^[41]

For our experiments, the polymer coating was removed from the sensing region of the optical fibre. When light propagates through the pure silica glass rod, it can be viewed as the core and the surrounding environment that the fibre optical sensors are embedded in (LFP/C65) forms the cladding of the pure silica glass rod. The evanescent wave produced through TIR events will hence be present at the totally reflecting interface between the pure silica fibre and the positive electrode soaked in electrolyte and can thus be used for evaluation of the cathode material. The changes in intensity during charge and discharge of an LFP–lithium half-cell using the RFO configuration is shown in Figure 2.

In this configuration, a gold mirror was coated at the end face of the optical fibre probe to allow the light to be reflected back to the detector. The in operando measurement in Figure 2 showed a clear correlation between the change in intensity with the charge and discharge of the LFP–lithium half-cells. Lithiation and delithiation of the positive electrode material results in a simultaneous change of attenuation of the intensity. The evanescent field extends into the surrounding electrode material soaked with electrolyte and the interaction results in modulation of the incident light in the optical fibre.

The change in intensity during cycling is more or less sigmoidal throughout charge and discharge with a small offset in the level of intensity depending on the wavelength. During charge the Li-ion concentration throughout the electrode decreases as the FePO_4 phase is formed and this results in an increase in intensity. During discharge, the Li-ion concentration in the positive electrode increase again as iron is reduced, forming LiFePO_4 . Consequently, the intensity decreases as can be seen in Figure 2d. This result is in good agreement with comparable optical studies on lithium iron phosphate which used a camera setup and indium tin oxide additives as electrochromic markers to study changes in reflectivity.^[15] From Figure S2a and b, the RFO–cell in Figure 2 shows a high coulombic efficiency and good capacity retention compared to the practical capacity of 150 mAh g^{-1} for the LiFePO_4 used in these experiments. This shows that the optical fibre sensor seems to have a minimal effect on the electrochemical performance of the cell.

A TFO configuration was also used to verify the results, see Figure 3. The change in intensity with charge and discharge for the TFO configuration is consistent with that obtained with the RFO configuration in Figure 2. In addition, the TFO configu-

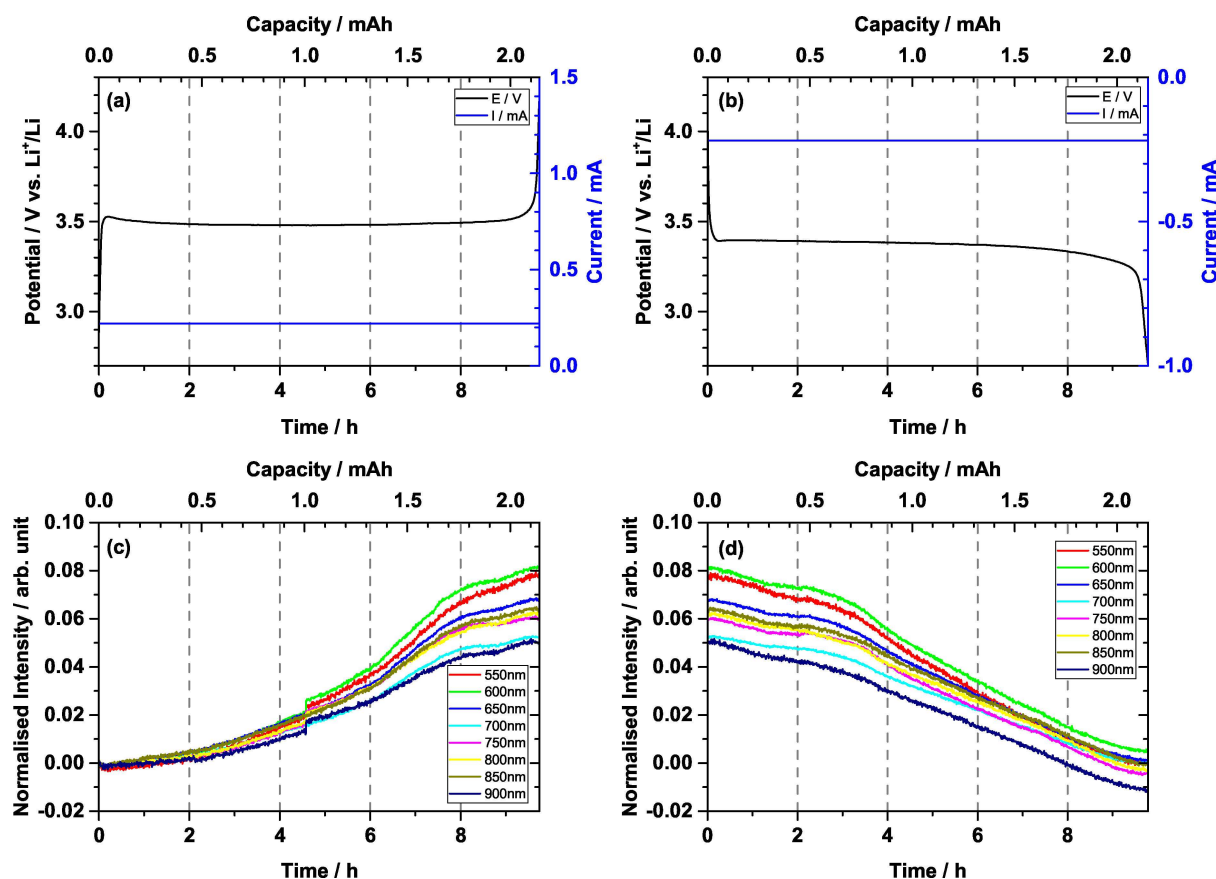


Figure 2. Constant current cycling of an LFP-lithium half-cell fitted with an optical fibre sensor in reflection configuration. The intensity is measured in real time while cycling the cell between 2.7 and 4.2 V vs. Li^+/Li . The applied current and voltage response as a function of time for one cycle during charge and discharge is shown in a) and b), respectively. The corresponding intensity change as a function of time and capacity during charge and discharge is shown in c) and d), respectively. Repeated cycles are presented in Figure S1.

ration (Figure 3) also shows that the optical response in the RFO measurement is not likely to originate from a potential plasmonic effect due to light interacting with the metallic mirror deposited at the end face of the fibre. The capacity retention and the coulombic efficiency for the TFO configuration (Figure S3a and b) is comparable with the RFO configuration. The overpotential seems, however, to increase faster with this setup, which could be attributed to a slightly more complicated cell design with the optical fibre entering and exiting the cell at two points rather than just one. As mentioned, the RFO sensor probe is favourable in this regard since it offers the advantage of being slightly easier to implement during battery assembly. However, the main advantage of TFO is the less complex optical setup with fewer contributions to uncertainties in optical signal and is thus chosen for the voltammetric experiments further below.

According to Equation (2), a longer wavelength should in theory result in a larger penetration depth of the evanescent field, which together with the number of ray reflections along the sensing region are related to the sensitivity of the sensor and ultimately the change in intensity. Other parameters that also affect the sensitivity include numerical aperture and the core radius of the fibre (the effect of the latter on sensitivity

depends on bending radius of the fibre).^[42] Since the penetration depth in Equation (2) is also a function of the refractive index of the fibre core and the surrounding medium, the absorption of evanescent waves could be influenced by changes in refractive index. In addition, it should be remembered that the refractive index of a medium varies with wavelength and could also be influenced by the temperature depending on the thermo-optic coefficient of the material. However, at the rather low (dis)charge rates used in the experiments and the efficient heat dissipation of the Swagelok cells, any temperature changes originating from the cycling are not expected to significantly influence the results. From the results in Figures 2 and 3, no clear correlation was found among the wavelengths and the intensities. Although the sigmoidal shape was similar, the absolute values of the intensities and the amplitude between full charge and discharge differed inconsistently (see Figure S5). Practical issues are likely also influencing the penetration depth. The applied pressure in the Swagelok during battery assembly is difficult to control precisely and will therefore influence the contact between the embedded fibre and the LFP/C65 particles, giving rise to variations in the evanescent field and hence the amount of light being attenuated.^[37] This is on the other hand expected to have

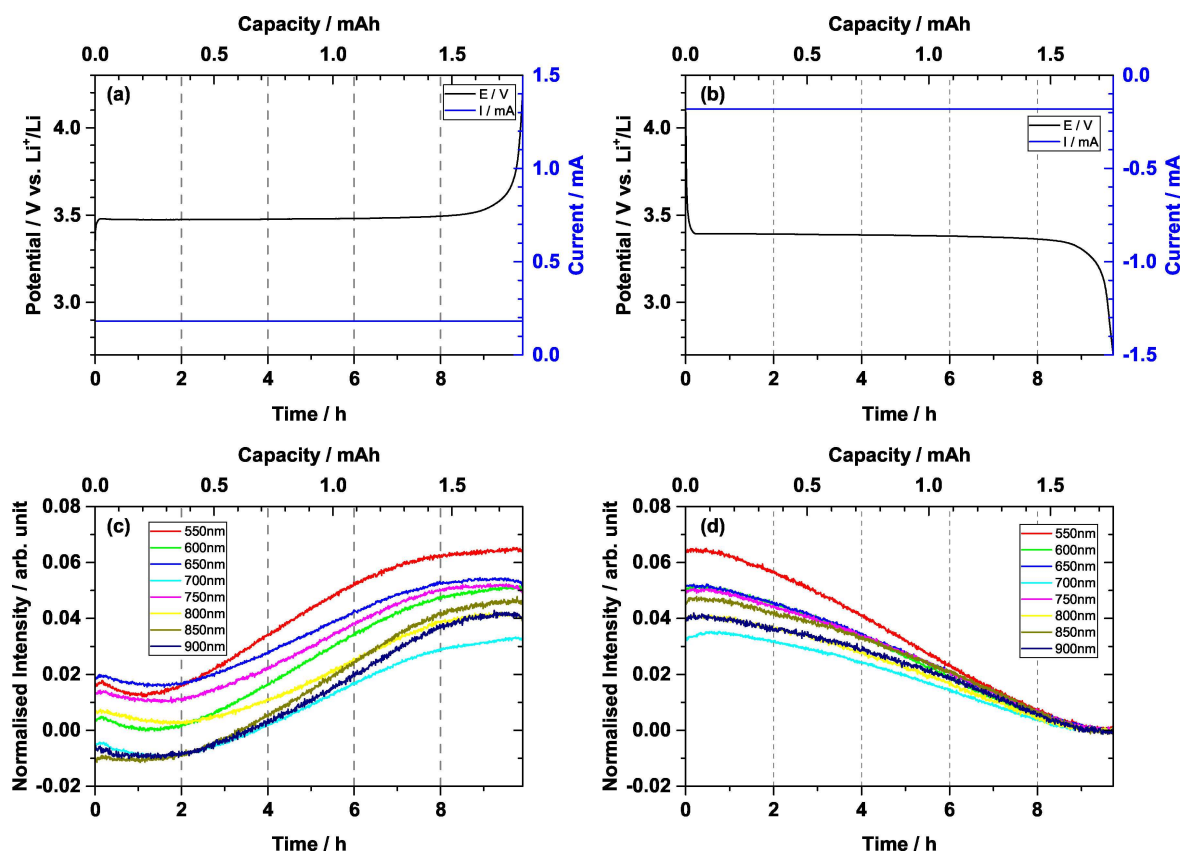


Figure 3. Constant current cycling of an LFP-lithium half-cell fitted with an optical fibre sensor in transmission configuration. The intensity is measured in real time while cycling the cell between 2.7 and 4.2 V vs. Li^+/Li . The applied current and voltage response as a function of time for one cycle is shown during charge and discharge in a) and b), respectively. The corresponding intensity change as a function of time and capacity during charge and discharge is shown in c) and d), respectively. Repeated cycles are presented in Figure S4.

a greater influence between experiments rather than between different wavelengths within an experiment. Another factor is any mechanical tension or bending of the optical fibre sensor. It has been shown in the literature^[34,36,43] that bending of a fibre optic sensor increases the loss of light and enhances the evanescent field and hence the sensitivity, a consequence of a decrease in the angle of incidence. Small bends or tensions caused by cell assembly could therefore influence the optical results over different wavelengths. Fibre bending has, in fact, been implemented to increase the sensitivity of optical sensors via increased penetration depths by giving them a U-shaped sensing region.^[36,41,44]

CV was performed with the TFO configuration to further verify the connection between the intensity changes and the charge and discharge of the LFP electrode. In a CV experiment, the (dis)charge is controlled by the potential, and the resulting current is linked to the number of iron oxidations/reductions (neglecting the double layer charging and any unwanted side-reactions). When the LFP is either fully charged or discharged the current drops to basically zero. This implies that the optical response should alternate between two levels and remain constant when the LFP is either fully charged or discharged. It should also be remembered that the charging/discharging rate is not constant in a CV experiment, as the current varies during

the experiment. As shown in Figure 4a, the CV experiment was performed between 2.7 and 4.2 V vs. Li^+/Li using a scan rate of $40 \mu\text{V s}^{-1}$, and shows as expected a distinct pair of current peaks per cycle, corresponding to oxidation (positive current) and reduction (negative current) of LFP. Starting from the left in Figure 4a, the current increases when the potential becomes sufficiently positive to oxidise more and more Fe^{2+} , while lithium ions are simultaneously extracted from the olivine structure. After a while, the current becomes mass transport limited, and gradually drops to nearly zero when all Fe^{2+} has been fully oxidised. The maximum oxidative current occurs around 3.63 V for both cycles shown in Figure 4 and during the reversed potential sweep, the reduction and the simultaneous insertion of Li ions in the delithiated FePO_4 phase gives a maximum reductive current at approximately 3.27 V.

The corresponding response from the optical fibre sensor is shown in Figure 4b, and it is clear that the intensity changes while the LFP is being oxidised or reduced. The intensity increases when the LFP is oxidised and returns to the same value after the following reduction, in line with the results in Figure 2 and 3 (constant current experiments). Figure 4b also demonstrates that, although the current gradually falls off after peak current has been reached, the intensity continues to increase until the oxidation is completed, and the reverse is

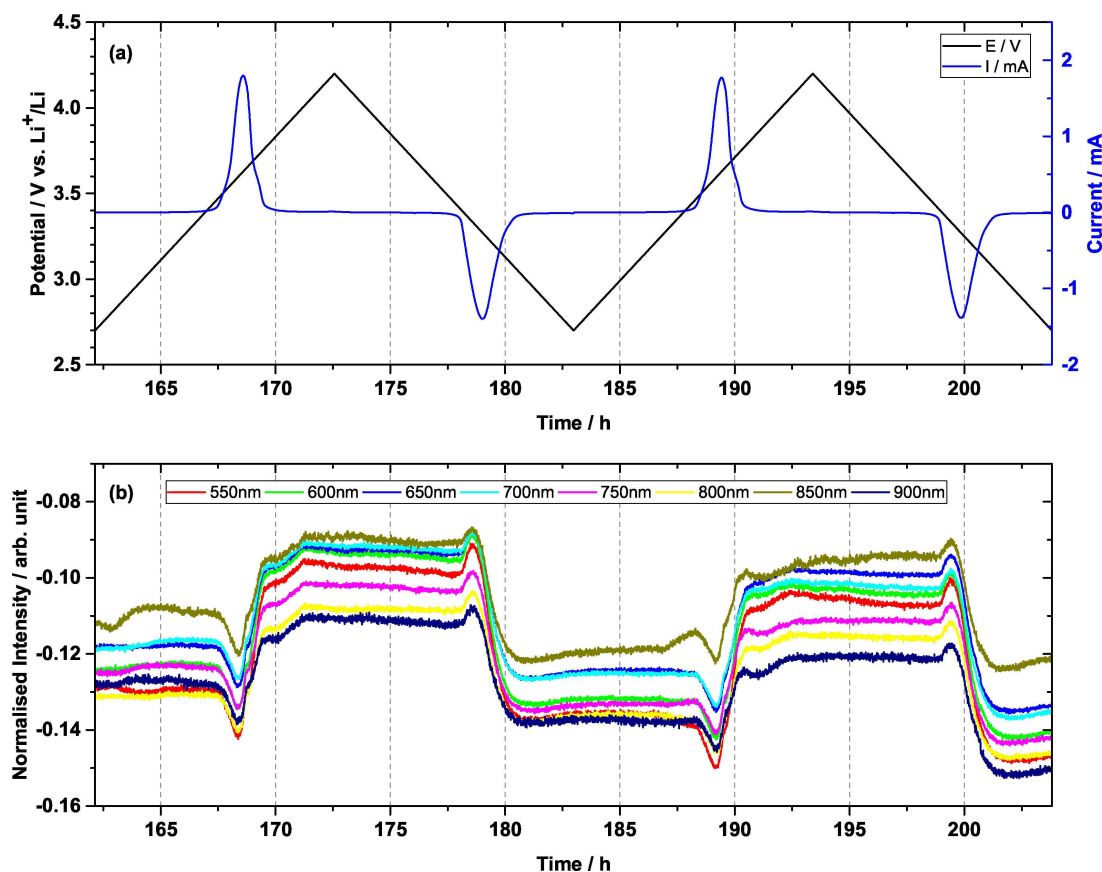


Figure 4. Two cycles of the CV experiment on an LFP-lithium half-cell fitted with an optical fibre in transmission configuration. The potential was scanned between 2.7 and 4.2 V vs. Li^+/Li with a scan rate of $40 \mu\text{V s}^{-1}$ and the intensity was measured simultaneously while cycling the cell. a) Applied potential and the current response. b) Corresponding intensity change as a function of time during oxidation and reduction of the positive electrode.

observed during reduction. A direct comparison with Figures 2 and 3 is, on the other hand, not straightforward due to the different time scales at which reactions proceed. With the present scan rate, almost all the capacity in the CV experiment during charge or discharge is obtained in about 2.5 h, compared to the constant current measurement that takes about 10 h.

What is also clear from Figure 4b is that there is a small initial decrease in the intensity when LFP begins to oxidise, and a corresponding small increase in the intensity at the onset of reduction. This can also be observed for the controlled current experiment in Figure 3. A comparison of the optical response from the cyclic voltammetry and the constant current measurement using the TFO configuration was made by plotting the intensity change during one cycle from each measurement as a function of capacity as can be seen in Figure S6 and Figure 3, respectively. To be able to compare the capacity and the corresponding optical response for both constant current and CV at the fixed time interval measured by the spectrometer, interpolation of the CV-data was performed. The interpolation points were set so that a capacity value was obtained for each data point recorded by the spectrometer. The resulting data is shown in Figure S6 and is thus a way to relate the intensity to the capacity in the CV experiments (similar to the controlled

current experiments). As mentioned above, there is an initial decrease in intensity during charge for both techniques. The intensity gently decreases to about 0.2–0.3 mAh for the constant current measurement (depending on the wavelength) and then increases throughout rest of the charge. The same initial decrease in intensity is present during charge (oxidation) in the CV with an initial decrease in intensity until about 0.5 mAh (which corresponds to about 28% SOC), followed by an increase throughout the rest of the oxidation. The reversed behaviour, although a bit less, is observed during the reduction (discharge). The intensity is initially increasing slightly until about 0.1 mAh, followed by a decrease in intensity throughout the rest of the discharge when using controlled current. The same is observed with the CV where the intensity increases slightly up to about 0.3 mAh followed by a decrease throughout the rest of the reduction. The reason for this behaviour is presently unknown, which warrants further investigations.

It has been shown in literature that LFP changes colour depending on the degree of lithiation and a slight colour change of the LFP in our experiments is thus expected during charge and discharge.^[45,46] Furthermore, other factors such as the particle size, synthesis route and presence of carbon coating are reported to influence the colour of LFP.^[46–48] Insertion and

extraction of lithium ions into the olivine structure changes the electronic structure of LiFePO_4 and its delithiated phase, which is related to the optical properties of the electrode material.^[49] Changes in the electronic state is often caused by mobile charge carriers such as electrons or holes that can absorb photons with energies within visible wavelengths leading to an electrochromic behaviour with distinct colour change.^[46] This was illustrated by Furutsuki et al., who studied the electrochromism of Li_xFePO_4 through diffuse reflectance and ab initio calculations and showed that inducing a $\text{Li}_{0.6}(\text{Fe}^{3+}_{1-x}\text{Fe}^{2+}_x\text{PO}_4)$ solid solution caused an increase in absorption around 650 nm, extending over the entire visible region.^[46] The increase in absorption was determined to be induced by intervalence charge transfer transition in the $\text{Fe}^{2+}/\text{Fe}^{3+}$ mixed valence state.^[46] In addition, diffuse reflectance measurements revealed an electrochromic reversibility between Li_xFePO_4 and FePO_4 where the colour was returned from chemically lithiated $\text{Li}_{0.6}\text{FePO}_4$ to FePO_4 . The colour of the sample was attributed to mixed valence state of $\text{Fe}^{2+}/\text{Fe}^{3+}$ and was reversible with Li-insertion into FePO_4 or extraction from Li_xFePO_4 . Besides a reversible electrochromic effect, the chemically lithiated $\text{Li}_{0.6}\text{FePO}_4$ also showed a higher absorption intensity compared to the delithiated FePO_4 which is in good agreement with the intensity changes between LiFePO_4 and FePO_4 observed with fibre optic sensors in our study. In addition, the samples showed low absorption across the visible and near-infrared region (500–900 nm) with small variation between wavelengths, which is in agreement with our result that show similar light intensity loss over all wavelengths throughout charge and discharge.

Diffuse reflectance spectroscopy was also employed by Zhang et al. to study the electronic band gap of LiFePO_4 and FePO_4 together with electron energy loss spectroscopy (EELS) and DFT calculations.^[50] The influence of coated or mechanically mixed carbon on the diffuse reflectance spectra of LFP was investigated and was found to increase the background absorption for both LiFePO_4 and FePO_4 as well as shift the absorption edge for LiFePO_4 to higher wavelengths (near infrared region). On the other hand, addition of carbon did not seem to significantly influence the absorption edge of the delithiated phase FePO_4 , implying sensitivity towards surface conditions.^[50] With this in mind, it is likely that the addition of carbon additives in our cells obscure optical observation of LFP as it increases background absorption, but a complete removal of carbon in battery electrodes is, nonetheless, not an alternative due to the poor electronic conductivity. In addition, Zhang et al. also found evidence of surface lithium depletion, which in conjunction with the influence of carbon additives on the diffuse reflectance spectra, indicated a surface related absorption.^[50] It was suggested that a solid solution $\text{Li}_x\text{Fe}^{3+}_{1-x}\text{Fe}^{2+}_x\text{PO}_4$ outer layer around the LiFePO_4 core is likely to cause energy absorption due to intervalence charge transfer transition^[47,50] as confirmed to occur experimentally for $\text{Li}_{0.6}(\text{Fe}^{3+}_{1-x}\text{Fe}^{2+}_x\text{PO}_4)$ solid solution.^[46] This should be compared with our results from the fibre optical sensors. The wavelength dependent penetration depth of the evanescent field at the sensor–electrode interface is in order of incident wavelengths and decreases exponentially with distance from the sensor surface.

This suggests that the optical response is most likely related to the surface condition of the LFP particles and the number of interactions along the sensing region.

Online estimation of state of charge using voltage in commercial lithium-ion batteries is challenging. The use of open circuit voltage to estimate SOC offers high accuracy but requires resting since it usually takes some time for battery cells to reach steady state and hence, cannot easily be used while an electrical vehicle is driving. In addition, the flat voltage profile of LFP makes it difficult to estimate SOC based on the cell voltage.^[5,6] As our result from the constant current and the cyclic voltammetry show, the integration of a fully embedded fibre optical sensor in the positive electrode could enable the continuous monitoring of state of charge in lithium-ion batteries. The sensor provides a consistent, repeatable and continuous change in intensity, which correlates well with state of charge throughout (dis)charge whereas the voltage plateau for LiFePO_4 remains unchanged. This offers valuable information about the electrode material not accessible through conventional temperature, current and voltage measurements from the battery. For the realisation and practical implementation of commercial fibre optical sensors in future LIBs several important steps need to be considered. These include simplifying and reducing costs for the optical equipment and components. Insertion of the optical fibres into battery electrodes would also have to be optimised not to damage sensors or electrodes as well as to minimise major changes to standard battery cell manufacturing. Obtaining a hermetic seal around the fibre at the input and output point of the cell will be crucial to avoid battery degradation from exposure to water and oxygen. Ultimately, the sensors have to be thoroughly characterised, optimised and calibrated with respect to the operating temperature and cell chemistry (i.e., the choice of battery material, additives and electrolyte). A sensor that could give complementary information could help to increase both the practical capacity and service life, as well as the possibility of early detection of safety issues in batteries. This is particularly relevant for positive electrode materials, which typically have a lower lithium storage capacity compared to most negative electrode materials and would thus ultimately limit the performance of lithium-ion batteries.

Conclusion

This paper demonstrates the implementation of fibre optic sensors and evanescent wave spectroscopy for real time optical monitoring of lithium-ion battery cells. The fibres were completely embedded in lithium iron phosphate and the experimental result were obtained over a wide range of wavelengths using two separate optical configurations. It was found that the results obtained from the reflection-based configuration were consistent with the transmission-based configuration. As shown with both constant current experiments and cyclic voltammetry (CV), the intensity correlated well with the cell capacity as the intensity increased upon charge as FePO_4 is formed and decreased upon discharge when lithium

ions were reinserted as LiFePO_4 forms again. CV provided further insight to the optical properties of the positive electrode material as the optical signal remained unchanged in the potential regions between the current peaks where the oxidative and reductive current is close to zero. In addition, CV (and to some extent also the constant current experiments) revealed an interesting variation in the intensity at the onset of oxidation and reduction of the lithium iron phosphate (LFP). Based on the results, embedded fibre optic sensors may be employed as an alternative indicator of state of charge (SOC) in battery cells. The optical signal correlates well with the SOC in the positive electrode in real time and is reproducible over multiple cycles. Furthermore, the optical signal does not rely on other commonly evaluated parameters in SOC estimation, such as current, voltage and temperature. Fibre optic sensors may also be useful for direct evaluation of the optical properties of materials relevant for energy storage.

Experimental Section

Electrode preparation and battery assembly

Commercial lithium iron phosphate (LFP-P2, Süd-Chemie) powder was used as active cathode material. The cathodes were prepared without any binder by mixing nanosized and carbon coated lithium iron phosphate with conductive carbon black (C-65, Imerys) in a weight ratio of 80:20. The electrode powder mixture was ball milled at 300 rpm for 30 min and subsequently dried at 120 °C for 24 h under vacuum prior to battery assembly. The negative electrodes consisted of 125 μm thick metallic lithium foil (Cyprus). LFP-lithium half-cells were assembled in order to isolate the optical observations to the positive electrode material only since graphite is known to change colour upon (de)lithiation.

It is well known that trace amounts of water present in the electrolyte or moisture introduced in leaky battery cells could cause decomposition of the widely used LiPF_6 salt or solvents, which lead to the formation of hydrofluoric acid (HF). The reactivity of HF towards SiO_2 , which the fibre sensors are made of, could damage their structural integrity, changing the optical signal over time. To exclude any changes in the optical signal due to etching of the fibre sensor, fluorine was removed from the customised fibre optic cells. Instead of using LiPF_6 commonly employed in commercial LIB electrolytes, an electrolyte based on Lithium bis(oxalato)borate (LiBOB) salt was used in a solvent mixture of ethylene carbonate (EC, BASF) and diethyl carbonate (DEC, Novolyte technologies). Likewise, the positive electrodes were prepared by mixing LiFePO_4 powder with conductive carbon black only, removing fluorinated binders such as PVDF completely. LiBOB (Chemetal) was dried at 120 °C for 24 h in a vacuum oven (Büchi) inside an argon filled glovebox (Mbraun) and then dissolved in a solvent mixture of EC/DEC in a ratio of 1:1 (v/v) to obtain a 0.8 M electrolyte. The EC/DEC mixture was dried with molecular sieves for about a week and the water content was subsequently determined to 4.5 ppm (obtained via Karl-Fischer titration).

LFP-lithium half-cells were assembled in custom modified Swagelok cells where fibre optic sensors were implemented as probes (reflection based) or inserted through the positive electrode (transmission based). The optical fibre sensors were inserted in the modified Swagelok cells through an opening at the side of the cell, in either of the two optical sensor configurations and then hermetically sealed by epoxy and a hot melt adhesive. The active

mass of the positive electrodes was about 14 mg of LiFePO_4 , and the fibre optic sensors were fully embedded in the positive electrode. Two pieces of glass fibre separator (Whatman™) were used in order to provide extra protection for the optical fibre once stack pressure was applied.

Electrochemical characterisation

Constant current cycling was performed in the range 2.7 to 4.2 V vs. Li^+/Li using either a VMP2 instrument (Biologic) or a LANHE CT2001A potentiostat. To minimise the risk of polarisation due to reduced particle contact, high mass loading or absence of binder and calendaring, a low applied current corresponding to 0.1 C (based on the active mass and a practical specific capacity of 150 mAh g^{-1}) was used during battery testing. Carbon additives were also added to the positive electrode to improve the electronic conductivity in the electrodes.

Cyclic voltammetry was performed using a VMP2 instrument (Biologic) with a scan rate of 40 $\mu\text{V s}^{-1}$. The scan rate was set so that the time for one cycle would roughly equal the time for one cycle at 0.1 C with constant current experiments. The LFP-lithium half-cells were also scanned between 2.7 and 4.2 V vs. Li^+/Li . All optical-electrochemical experiments were performed in a cleanroom environment with a controlled room temperature of 21 ± 1 °C.

Optical sensor setup and characterisation

The optical-electrochemical sensor setup consists of a computer connected to a commercially available optics unit (Insplorion AB) equipped with a tungsten-halogen light source and a Vis/NIR-spectrometer as seen in the schematic in Figure 1. The fibre optic sensors were prepared by splicing two standard step index multimode optical fibre pigtailed (FG105LCA, Thorlabs) with core diameter 105.5 μm and cladding diameter 125 μm to both ends of a coreless optical fibre (FG125LA, Thorlabs) of 125 μm in diameter and 12 mm in length using a fusion splicer (FITELNINJA NJ001). The polymer coating of the multimode optical fibre pigtailed was removed mechanically with a fibre stripper and the ends were cut using a high precision cleaver (FITEL S326 A) prior to splicing. The sensing region is based on a coreless optical fibre, which is a pure silica glass rod with a polymer coating, where the polymer coating was softened using acetone and removed mechanically with a fibre stripper. This allows the evanescent field present at the interface between the pure silica glass rod and the positive electrode soaked in electrolyte to interact with the LFP-particles. White light was launched into the waveguide with a tungsten-halogen light source and optical data was collected in operando with the spectrometer while cycling the batteries. If a reflection-based fibre optic sensor configuration is used, a fibre optic beam splitter (OZ Optics LTD) is required to couple the light in and out of the fibre optic sensor. Fibre sensors used as reflection-based probes also had a gold mirror deposited at the end face of the fibre in order to increase the reflection of light in the fibre back to the detector. In transmission configuration, there is no need for a fibre optic beam splitter. Spectra were recorded by a charge coupled device (CCD) detector using wavelengths in the visible near-infrared band (550–900 nm). The collected spectra were subtractively normalised according to $\Delta I/I_0 = (I - I_0)/I_0$, where I is the intensity measured continuously throughout cycling at each wavelength and I_0 the intensity at each wavelength when the electrode was fully discharged during first cycle.

Acknowledgements

The EU-projects LiRichFCC (project number 711792) and SintBat (project number 685716) are acknowledged for financial support. StandUp for Energy and Skellefteå Kraft are also gratefully acknowledged for financial support.

Conflict of Interest

The authors declare no conflict of interest.

Keywords: cyclic voltammetry · evanescent wave · lithium iron phosphate · lithium-ion batteries · sensors

- [1] N. Nitta, F. Wu, J. T. Lee, G. Yushin, *Mater. Today* **2015**, *18*, 252–264.
- [2] C. P. Grey, J. M. Tarascon, *Nat. Mater.* **2017**, *16*, 45–56.
- [3] J.-M. Tarascon, M. Armand, *Nature* **2001**, *414*, 359–367.
- [4] S. M. Rezvanianiani, Z. Liu, Y. Chen, J. Lee, *J. Power Sources* **2014**, *256*, 110–124.
- [5] L. Lu, X. Han, J. Li, J. Hua, M. Ouyang, *J. Power Sources* **2013**, *226*, 272–288.
- [6] W. Waag, C. Fleischer, D. U. Sauer, *J. Power Sources* **2014**, *258*, 321–339.
- [7] J. B. Goodenough, K.-S. Park, *J. Am. Chem. Soc.* **2013**, *135*, 1167–1176.
- [8] J. Vetter, P. Novák, M. R. Wagner, C. Veit, K.-C. Möller, J. O. Besenhard, M. Winter, M. Wohlfahrt-Mehrens, C. Vogler, A. Hammouche, *J. Power Sources* **2005**, *147*, 269–281.
- [9] A. Urrutia, J. Goicoechea, F. J. Arregui, *J. Sens.* **2015**, *2015*, 1–18.
- [10] B. Lee, *Opt. Fiber Technol.* **2003**, *9*, 57–79.
- [11] K. T. V. Grattan, T. Sun, *Sens. Actuators A* **2000**, *82*, 40–61.
- [12] L. Xie, J. Lu, *J. Electroanal. Chem.* **2001**, *497*, 159–162.
- [13] P. Maire, H. Kaiser, W. Scheifele, P. Novák, *J. Electroanal. Chem.* **2010**, *644*, 127–131.
- [14] S. J. Harris, A. Timmons, D. R. Baker, C. Monroe, *Chem. Phys. Lett.* **2010**, *485*, 265–274.
- [15] V. Roscher, F. Rittweger, K.-R. Riemschneider, *ACS Appl. Mater. Interfaces* **2019**, *11*, 6900–6906.
- [16] A. Raghavan, P. Kiesel, L. W. Sommer, J. Schwartz, A. Lochbaum, A. Hegyi, A. Schuh, K. Arakaki, B. Saha, A. Ganguli, K. H. Kim, C. Kim, H. J. Hah, S. Kim, G.-O. Hwang, G.-C. Chung, B. Choi, M. Alamgir, *J. Power Sources* **2017**, *341*, 466–473.
- [17] A. Ganguli, B. Saha, A. Raghavan, P. Kiesel, K. Arakaki, A. Schuh, J. Schwartz, A. Hegyi, L. W. Sommer, A. Lochbaum, S. Sahu, M. Alamgir, *J. Power Sources* **2017**, *341*, 474–482.
- [18] L. W. Sommer, A. Raghavan, P. Kiesel, B. Saha, J. Schwartz, A. Lochbaum, A. Ganguli, C.-J. Bae, M. Alamgir, *J. Electrochem. Soc.* **2015**, *162*, A2664–A2669.
- [19] C.-J. Bae, A. Manandhar, P. Kiesel, A. Raghavan, *Energy Technol.* **2016**, *4*, 851–855.
- [20] L. W. Sommer, P. Kiesel, A. Ganguli, A. Lochbaum, B. Saha, J. Schwartz, C.-J. Bae, M. Alamgir, A. Raghavan, *J. Power Sources* **2015**, *296*, 46–52.
- [21] T. Amietszajew, E. McTurk, J. Fleming, R. Bhagat, *Electrochim. Acta* **2018**, *263*, 346–352.
- [22] A. Gaston, I. Lozano, F. Perez, F. Auza, J. Sevilla, *IEEE Sens. J.* **2003**, *3*, 806–811.
- [23] S. Azad, E. Sadeghi, R. Parvizi, A. Mazaheri, M. Yousefi, *Opt. Laser Technol.* **2017**, *90*, 96–101.
- [24] Z. Zhao, Y. Duan, *Sens. Actuators B* **2011**, *160*, 1340–1345.
- [25] S. Dong, M. Luo, G. Peng, W. Cheng, *Sens. Actuators B* **2008**, *129*, 94–98.
- [26] W. Cao, Y. Duan, *Sens. Actuators B* **2005**, *110*, 252–259.
- [27] B. Renganathan, D. Sastikumar, R. Srinivasan, A. R. Ganesan, *Mater. Sci. Eng. B* **2014**, *186*, 122–127.
- [28] B. Renganathan, D. Sastikumar, G. Gobi, N. R. Yogamalar, A. C. Bose, *Sens. Actuators B* **2011**, *156*, 263–270.
- [29] Q. Yan, S. Tao, H. Toghiani, *Talanta* **2009**, *77*, 953–961.
- [30] N. Matsuyama, S. Okazaki, H. Nakagawa, H. Sone, K. Fukuda, *Thin Solid Films* **2009**, *517*, 4650–4653.
- [31] A. Ghannoum, R. C. Norris, K. Iyer, L. Zdravkova, A. Yu, P. Nieva, *ACS Appl. Mater. Interfaces* **2016**, *8*, 18763–18769.
- [32] A. Ghannoum, P. Nieva, A. Yu, A. Khajepour, *ACS Appl. Mater. Interfaces* **2017**, *9*, 41284–41290.
- [33] A. Ghannoum, P. Nieva, *J. Energy Storage* **2020**, *28*, 101233.
- [34] A. Leung, P. M. Shankar, R. Mutharasan, *Sens. Actuators B* **2007**, *125*, 688–703.
- [35] A. R. Hind, S. K. Bhargava, A. McKinnon, *Adv. Colloid Interface Sci.* **2001**, *93*, 91–114.
- [36] N. Punjabi, J. Satija, S. Mukherji in *Sensing Technology: Current Status and Future Trends III* (Eds.: A. Mason, S. C. Mukhopadhyay, K. P. Jayasundera), Springer International Publishing, Cham, **2015**, pp. 25–45.
- [37] M. Milosevic, *Appl. Spectrosc. Rev.* **2004**, *39*, 365–384.
- [38] M. Ahmad, L. L. Hench, *Biosens. Bioelectron.* **2005**, *20*, 1312–1319.
- [39] V. Ruddy, B. D. MacCraith, J. A. Murphy, *J. Appl. Phys.* **1990**, *67*, 6070–6074.
- [40] L.-K. Chau, Y.-F. Lin, S.-F. Cheng, T.-J. Lin, *Sens. Actuators B* **2006**, *113*, 100–105.
- [41] B. D. Gupta, H. Dodeja, A. K. Tomar, *Opt. Quantum Electron.* **1996**, *28*, 1629–1639.
- [42] S. K. Khijwania, B. D. Gupta, *Opt. Quantum Electron.* **1999**, *31*, 625–636.
- [43] B. D. Gupta, R. Kant, *Opt. Laser Technol.* **2018**, *101*, 144–161.
- [44] P. Nath, *Microw. Opt. Technol. Lett.* **2009**, *51*, 3004–3006.
- [45] A. Yamada, *Electrochemistry* **2016**, *84*, 654–661.
- [46] S. Furutsuki, S.-C. Chung, S. Nishimura, Y. Kudo, K. Yamashita, A. Yamada, *J. Phys. Chem. C* **2012**, *116*, 15259–15264.
- [47] Y. Zhang, J. A. Alarco, J. Y. Nerkar, A. S. Best, G. A. Snook, P. C. Talbot, B. C. C. Cowie, *ACS Appl. Energy Mater.* **2020**, *3*, 2856–2866.
- [48] M. M. Doeff, J. D. Wilcox, R. Kostecki, G. Lau, *J. Power Sources* **2006**, *163*, 180–184.
- [49] K. Zaghib, A. Mauger, J. B. Goodenough, F. Gendron, C. M. Julien, *Chem. Mater.* **2007**, *19*, 3740–3747.
- [50] Y. Zhang, J. A. Alarco, A. S. Best, G. A. Snook, P. C. Talbot, J. Y. Nerkar, *RSC Adv.* **2019**, *9*, 1134–1146.

Manuscript received: June 14, 2020
 Revised manuscript received: August 14, 2020
 Accepted manuscript online: August 21, 2020
 Version of record online: September 9, 2020